ECCOMAS Congress 2016
VII European Congress on Computational Methods in Applied Sciences and Engineering
M. Papadrakakis, V. Papadopoulos, G. Stefanou, V. Plevris (eds.)
Crete Island, Greece, 5–10 June 2016

MANIFESTATION OF ASCENDANCY OF EXTINCTION-REIGNITION ON SOUNDING HYBRID ROCKET USING DESIGN INFORMATICS

Kazuhisa Chiba[1], **Masahiro Kanazaki**[2], **and Toru Shimada**[3]

[1]The University of Electro-Communications
1-5-1, Chofugaoka, Chofu, Tokyo 182-8585, Japan
e-mail: kazchiba@uec.ac.jp

[2] Tokyo Metropolitan University
6-6, Asahigaoka, Hino, Tokyo 191-0065, Japan
e-mail: kana@tmu.ac.jp

[3] Japan Aerospace Exploration Agency
3-1-1, Yoshinodai, Chuo, Sagamihara 252-5210, Japan
e-mail: shimada.toru@jaxa.jp

Keywords: Extinction-Reignition, Sounding Launch Vehicle, Hybrid Rocket Engine, Design Informatics, Multidisciplinary Design Optimization, Data Mining.

Abstract. *Information visualization have been performed for researching and developing a single-stage sounding launch vehicle with hybrid rocket engine by using design informatics; it has three points of view: problem definition, optimization, and data mining. The primary objective of this study is to reveal extinction-reignition ascendancy, which is one of the beneficial points of hybrid rocket, for expanding downrange and duration in the lower thermosphere. Swirling-flow oxidizer is furnished with solid fuel; we adopt polypropylene for solid fuel and liquid oxygen for oxidizer. A multidisciplinary design optimization was implemented by using a hybrid evolutionary computation; data mining was carried out by using a scatter plot matrix to efficiently perceive the entire design space. It is consequently revealed that extinction-reignition extends duration although it does not provide any effect on expanding downrange. Scatter plot matrix results express physical mechanisms of design-variable behaviors for the objective functions and also the roles of the design variables via bird's-eye visualization of the entire design-space constitution.*

1 INTRODUCTION

Single-stage rockets have been researched and developed for scientific observations and experiments of high-altitude zero-gravity condition, whereas multi-stage rockets have been for orbit injections of payloads. Institute of Space and Astronautical Science (ISAS)/Japan Aerospace Exploration Agency (JAXA) has been operating Kappa, Lambda, and Mu series rockets as the representatives of solid rocket to contribute to space science researches. Although Epsilon series began to be operated from September 2013, a next-generation rocket is necessary to fulfill higher-frequent and lower-cost space transportations.

Hybrid rocket engines (HREs) using different phases between fuel and oxidizer (solid fuel and liquid/gas oxidizer is generally used) have been researched and developed as an innovative technology in mainly the E.U.[1] and the U.S.[2] Each country has plans to adopt an HRE to a main engine of space transports because of several advantages: lower cost, higher safety[1], and pollution free flight due to no gunpowder use. In contrast, disadvantages of HREs proceed from their combustion. Since HREs have low regression rate of solid fuel due to turbulent boundary layer combustion, the thrust of HREs is less than that of pure-solid/liquid engines which premixed combustion[3] is implemented. Moreover, since the mixture ratio between solid fuel and liquid/gas oxidizer (O/F) is temporally fluctuated, thrust changes with time. Research topics of HREs are improving those performances via experiments.

Now in Japan, ISAS/JAXA recently researches HREs to develop a next-generation space transportation. Research topics are viporization of liquid oxygen, advancement of exhaust velocity c^* efficiency, progress of regression rate, stable ignition, and numerical simulations of turbulent boundary layer combustion. In contrast, we will investigate hybrid-rocket ascendancy via conceptual design as a part of ISAS/JAXA's hybrid rocket project. The objective of this conceptual design is to quantitatively indicate hybrid-rocket advantage compared with the current rockets via conceptual design; multidisciplinary design requirements: chemical equilibrium, thrust, structural, aerodynamics, and trajectory analyses are driven. Furthermore, exhaustive design information will be obtained to additionally consider manufacturing, productive, and market factors for practical problems[2].

Design informatics (DI) has essential for not only an operating system itself but also its applications to practical problems so that science contributes toward the real world. Results themselves do not possess versatility in application problems due to their particularity; system versatility is indeed critical in application problems because it is revealed that application range is expanded. Furthermore, the application results indicate the guidance for system improvements. In this study, we conceptually explore a conceptual design of a single-stage sounding hybrid rocket using DI approach. The objective is that extinction-reignition advantage in the science mission for aurora observation on hybrid rocket will be quantitatively revealed. Since HREs are comparatively easy to perform multi-time ignition[4], extinction-reignition supremacy is especially predicted by using design informatics approach.

We researched step by step in the previous studies. As a first step, an optimization problem on single-time ignition, which is the identical condition of the current solid rocket, was defined to obtain the design information[5]. As a second step, the implication of solid fuels in the performance of hybrid rocket was revealed because the regression rate is one of the key elements for hybrid-rocket performance[6]. Finally, this study investigates an extinction-reignition sequence to reveal a hybrid-rocket ascendancy as multi-time ignition.

[1] this is especially important for manned mission.

[2] optimization is difficult to deal with them due to the difficulty of quantitative definition.

Table 1: Upper/lower limits of each design variable.

serial number	*design variable*	*unit*	*design space*		
dv1	initial mass flow of oxidizer	[kg/sec]	$1.0 \leq$	$\dot{m}_{\mathrm{ox}}(0)$	≤ 30.0
dv2	fuel length	[m]	$1.0 \leq$	L_{fuel}	≤ 10.0
dv3	initial radius of port	[m]	$0.01 \leq$	$r_{\mathrm{port}}(0)$	≤ 0.30
dv4	total combustion time	[sec]	$20.0 \leq$	$t_{\mathrm{burn}}^{(\mathrm{total})}$	≤ 60.0
dv5	1st combustion time	[sec]	$10.0 \leq$	$t_{\mathrm{burn}}^{(\mathrm{1st})}$	≤ 40.0
dv6	extinction time	[sec]	$1.0 \leq$	t_{ext}	≤ 300.0
dv7	initial pressure in combustion chamber	[MPa]	$3.0 \leq$	$P_{\mathrm{cc}}(0)$	≤ 6.0
dv8	aperture ratio of nozzle	[-]	$5.0 \leq$	ϵ	≤ 8.0
dv9	elevation at launch time	[deg]	$60.0 \leq$	$\phi(0)$	≤ 90.0

The constitution of this paper is as follows. The optimization and data-mining techniques used in DI are explained in Chapter II. The problem definition for designing a hybrid rocket are shown in Chapter III. Otimization and data-mining results are revealed; the knowledge is also discussed in Chapter IV.

2 PROBLEM DEFINITION

We consider a conceptual design for a single-stage sounding hybrid rocket, simply composed of a payload chamber, an oxidizer tank, a combustion chamber, and a nozzle[7] shown in Fig. 1. A launch vehicle for aurora scientific observation will be focused because more efficient sounding rockets are desired due to successful obtaining new scientific knowledge on the aurora observation by ISAS/JAXA in 2009. In addition, a single-stage hybrid rocket problem fits for resolving fundamental physics regarding HREs and for improving the problem definition.

2.1 Objective functions

Three objective functions are defined. First objective is maximizing the downrange in the lower thermosphere (altitude of 90 to 150 [km]) R_d [km] (obj1). Second is maximizing the duration in the lower thermosphere T_d [sec] (obj2). It recently turns out that atmosphere has furious and intricate motion in the lower thermosphere due to energy injection, from which derives aurora, from high altitude. The view of these objective functions is to secure the hor-

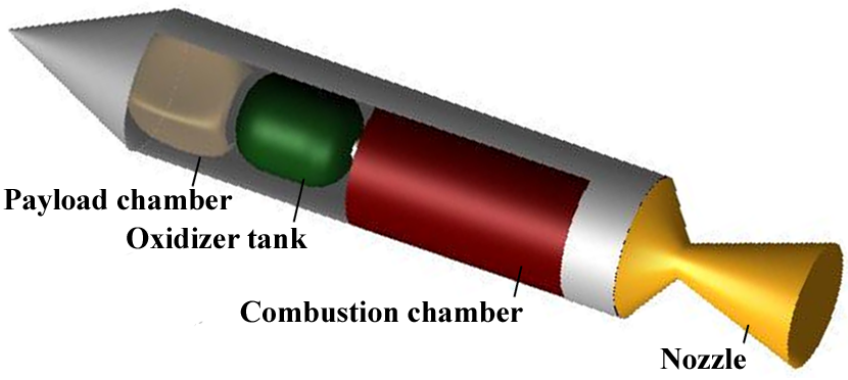

Figure 1: Conceptual illustrations of hybrid rocket.

izontal distance and time for competently observing atmospheric temperature and the wind so that thermal energy balance is elucidated on atmospheric dynamics. Third objective is minimizing the initial gross weight of launch vehicle $M_{\text{tot}}(0)$ [kg] (obj3), which is generally the primary proposition for space transportations.

2.2 Design variables

We use nine design variables: initial mass flow of oxidizer $\dot{m}_{\text{ox}}(0)$ [kg/sec] (dv1), fuel length L_{fuel} [m] (dv2), initial radius of port $r_{\text{port}}(0)$ [m] (dv3), total combustion time $t_{\text{burn}}^{(\text{total})}$ [sec] (dv4), first combustion time $t_{\text{burn}}^{(1\text{st})}$ [sec] (dv5), extinction time from the end of first combustion to the beginning of second combustion t_{ext} [sec] (dv6), initial pressure in combustion chamber $P_{\text{cc}}(0)$ [MPa] (dv7), aperture ratio of nozzle ϵ [-] (dv8), and elevation at launch time $\phi(0)$ [deg] (dv9). The design variables regarding rocket geometry are visualized in Fig. 2.

Note that since this problem assumes

$$\dot{m}_{\text{ox}}(t) = \dot{m}_{\text{ox}}(0) = \text{const.}, \tag{1}$$

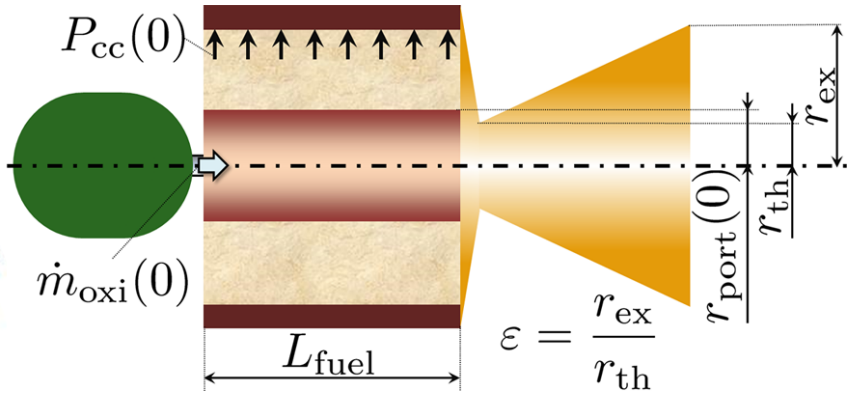

Figure 2: Design variables regarding rocket geometry. ϵ is described by using the radius at nozzle exit r_{ex} and the radius at nozzle throat r_{th}.

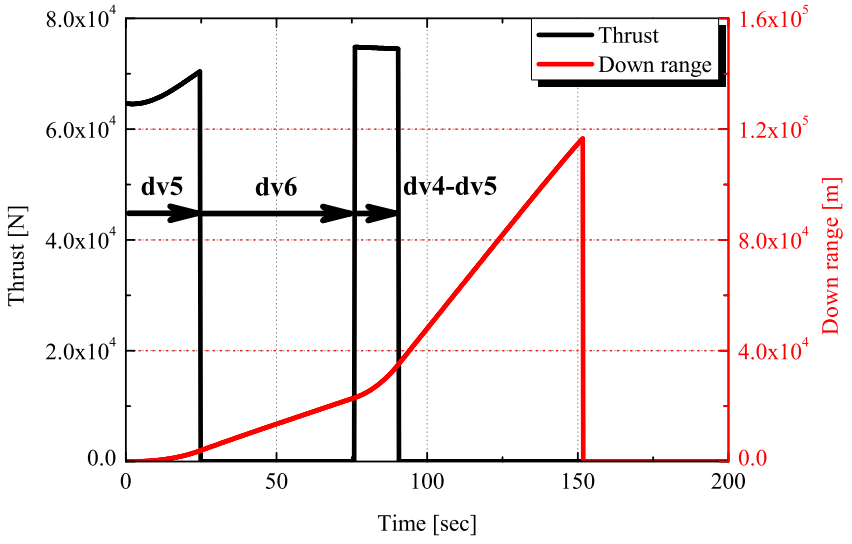

Figure 3: Conceptual graph of extinction-reignition. Two-time combustions generate two thrust pulses. Second thrust pulse increases $\mathrm{d}R_d/\mathrm{d}t$.

mass flow of oxidizer is equal between 1st and 2nd combustions. The relationship among dv4, dv5, and dv6 regarding extimction-reignition operation is conceptually shown in Fig. 3. We set two combustion times as follows:

$$
\begin{aligned}
t_{\text{burn}}^{(\text{1st})} &= \begin{cases} t_{\text{burn}}^{(\text{total})} & (t_{\text{burn}}^{(\text{total})} < t_{\text{burn}}^{(\text{1st})}) \\ t_{\text{burn}}^{(\text{1st})} & (t_{\text{burn}}^{(\text{total})} \geq t_{\text{burn}}^{(\text{1st})}) \end{cases}, \\
t_{\text{burn}}^{(\text{2nd})} &= \begin{cases} 0 & (t_{\text{burn}}^{(\text{total})} < t_{\text{burn}}^{(\text{1st})}) \\ t_{\text{burn}}^{(\text{total})} - t_{\text{burn}}^{(\text{1st})} & (t_{\text{burn}}^{(\text{total})} \geq t_{\text{burn}}^{(\text{1st})}) \end{cases}.
\end{aligned}
\tag{2}
$$

Under $t_{\text{burn}}^{(\text{total})} < t_{\text{burn}}^{(\text{1st})}$ condition, it is defined that $t_{\text{burn}}^{(\text{1st})}$ is set to be $t_{\text{burn}}^{(\text{total})}$ and second-time combustion is not performed. Note that there is no constraint except upper/lower limits of each design variable summarized in Table 1. These upper/lower values are exhaustively covering the region of the design space which is physically admitted. When there is a sweet spot[3] in the objective-function space, the exploration space would intentionally become narrow due to the operation of range adaptation on the evolutionary computation.

2.3 Evaluation method of hybrid rocket

First of all, $O/F(t)$ is computed by the following equation.

$$
O/F(t) = \frac{\dot{m}_{\text{ox}}(t)}{\dot{m}_{\text{fuel}}(t)}, \tag{3}
$$

where, $\dot{m}_{\text{ox}}(t)$ is set from eq. (1) and

$$
\begin{aligned}
\dot{m}_{\text{fuel}}(t) &= 2\pi r_{\text{port}}(t) L_{\text{fuel}} \rho_{\text{fuel}} \bar{\dot{r}}_{\text{port}}(t), \\
r_{\text{port}}(t) &= r_{\text{port}}(0) + \int \dot{r}_{\text{port}}(t) \mathrm{d}t.
\end{aligned}
\tag{4}
$$

$\dot{m}_{\text{ox}}(t)$ and $\dot{m}_{\text{fuel}}(t)$ are the mass flow of oxidizer/fuel [kg/sec] at time t, respectively. $r_{\text{port}}(t)$ is port radius [m] at t, L_{fuel} describes fuel length, and ρ_{fuel} is fuel density [kg/m^3]. $\dot{r}_{\text{port}}(t)$ describes the regression rate. Note that since HREs perform no premixed combustion which conventional rocket engine implements but turbulent boundary layer combustion, $O/F(t)$ is not constant but timely fluctuated. After that, an analysis of chemical equilibrium is performed by using NASA-CEA (chemical equilibrium with applications) [8], then trajectory, thrust, aerodynamic, and structural analyses are respectively implemented. A body is assumed as rigidness. As the time step is set to be 0.5 [sec], it takes roughly 10 [sec] for an individual evaluation on a general desktop computer.

A combustion chamber is filled with solid fuel with a single port at the center to supply oxidizer. As the regression rate to the radial direction $\dot{r}_{\text{port}}(t)$ [m/sec] generally governs thrust power of HREs, it is a significant parameter. This study uses the following experimental model[9, 10];

$$
\begin{aligned}
\dot{r}_{\text{port}}(t) &= a_{\text{fuel}} \times G_{\text{ox}}^{n_{\text{fuel}}}(t) \\
&= a_{\text{fuel}} \times \left(\frac{\dot{m}_{\text{ox}}(t)}{\pi r_{\text{port}}^2(t)} \right)^{n_{\text{fuel}}},
\end{aligned}
\tag{5}
$$

[3] the region that all objective functions proceed optimum directions.

where, $G_{\mathrm{ox}}(t)$ is oxidizer mass flux [kg/m^2/sec]. a_{fuel} [m/sec] and n_{fuel} [-] are the constant values experimentally determined by fuels. Swirling oxidizer flow is carried out; we adopt liquid oxygen for oxidizer and polypropylene as thermoplastic resin for solid fuel. Experiments[9, 10] respectively indicate $a_{\mathrm{fuel}} = 8.26 \times 10^{-5}$ [m/sec] and $n_{\mathrm{fuel}} = 0.5500$ [-] for polypropylene.

We assume a body to be rigid[11]. Figure 4 shows a three-degree-of-freedom (3DoF) flight simulation kinematic model. $T(t)$ is estimated; a flight path is computed by using the following 3DoF equations of motion:

$$\begin{cases} \ddot{x} = \dfrac{T(t)\cos\theta_1 - D(t)\cos\theta_2}{M_{\mathrm{tot}}(t)}, \\ \ddot{y} = \dfrac{T(t)\sin\theta_1 - D(t)\sin\theta_2}{M_{\mathrm{tot}}(t)} - g, \\ \ddot{\theta}_1 = \dfrac{N(t)|X_{\mathrm{c.p.}} - X_{\mathrm{c.g.}}|}{I(t)}, \end{cases} \tag{6}$$

where, $N(t)$ is the normal component of aerodynamic force. $N(t)$ is approximately evaluated as follows:

$$N(t) = \frac{1}{2}\rho(t)V^2(t)S_{\mathrm{ref}}\sin(|\theta_1 - \theta_2|). \tag{7}$$

$\rho(t)$ and $V(t)$ respectively denote the air density and rocket velocity at elapsed time t. θ_1 and θ_2 respectively describe vehicle attitude angle and flight path angle. Eq. 6 assumes that thrust vector corresponds to attitude direction, i.e., body axis. Therefore, thrust angle does not generally correspond to flight direction. $I(t)$ denotes the moment of inertia, which is estimated by using the coordinate of the center of gravity for an entire body $X_{\mathrm{c.g.}}(t)$ and that for the

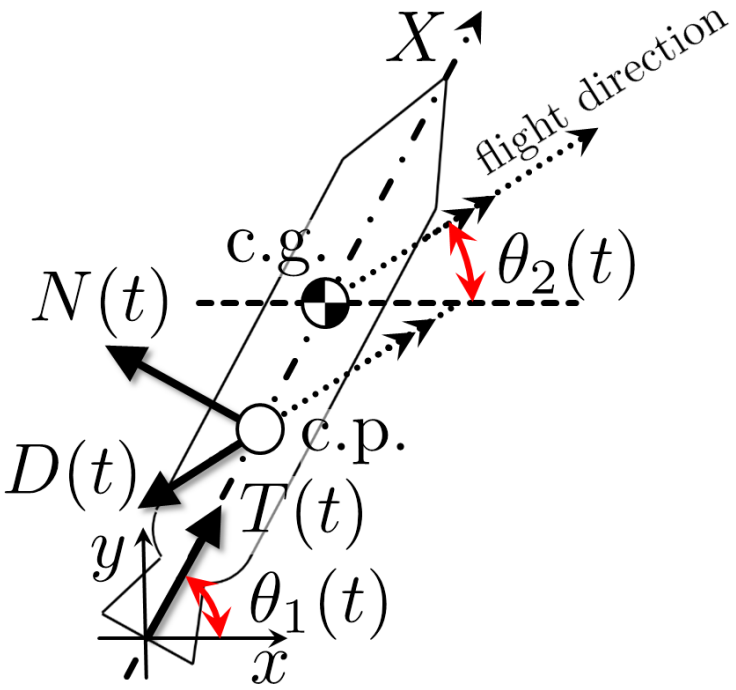

Figure 4: Illustration of a kinematic model of single-stage rocket for 3DoF flight simulation. Note that c.g. and c.p. respectively denote the center of gravity and the center of pressure.

components of body $X_{\text{c.g.}}^{(n\_\text{comp})}(t)$ shown in Fig. 5; $I(t)$ is described as follows:

$$I(t) = \sum_{n\_\text{comp}=1}^{5} m_{n\_\text{comp}}(t) \times (X_{\text{c.g.}}^{(n\_\text{comp})}(t) - X_{\text{c.g.}}(t))^2. \tag{8}$$

$X_{\text{c.g.}}$ is computed by the following equation, which considers the variance of fuel and oxidizer masses.

$$X_{\text{c.g.}}(t) = \sum_{n\_\text{comp}=1}^{5} \frac{m_{n\_\text{comp}}(t) \times X_{\text{c.g.}}^{(n\_\text{comp})}(t)}{M_{\text{tot}}(t)}. \tag{9}$$

$X_{\text{c.g.}}^{(n\_\text{comp})}(t)$ describes the distance between nozzle exit and the center of gravity of each component. $n_$comp denotes the serial number of each component; we consider five components. $n_$comp of 1, 2, 3, 4, and 5 respectively correspond to nozzle, combustion chamber, oxidizer tank, payload bay, and nose cone. Note that $m_{n\_\text{comp}}(t)$ for nozzle, payload bay, and nose cone merely depends on the structures of these components; $m_{n\_\text{comp}}(t)$ can be assumed to be constant. In contrast, $m_{n\_\text{comp}}(t)$ for combustion chamber and oxidizer tank depends on not only the structure but also change in the amount of fuel and oxidizer over time. That is, $X_{\text{c.g.}}^{(2)}(t)$ and $X_{\text{c.g.}}^{(3)}(t)$ are time-dependent functions. $M_{\text{tot}}(t)$ denotes the total mass for a whole rocket body.

3 DESIGN INFORMATICS

DI is essential for practical design problems. Although solving design optimization problems is important under many-discipline consideration on engineering[12], the most significant part of the process is the extraction of useful knowledge of the design space from results of optimization runs[13, 14]. The results produced by multiobjective optimization (MOO) are not an individual optimal solution but rather an entire set of optimal solutions due to tradeoffs. That is, MOO results are not sufficient from the practical point of view as designers need a conclusive shape and not the entire selection of possible optimal shapes. But optimal-solution set produced by an MOO can be considered a hypothetical design database for design space. Thereupon, data mining techniques can be applied to a hypothetical database to acquire not only useful design knowledge but also structurizing and visualizing design space for conception support. This approach was suggested as DI[15].

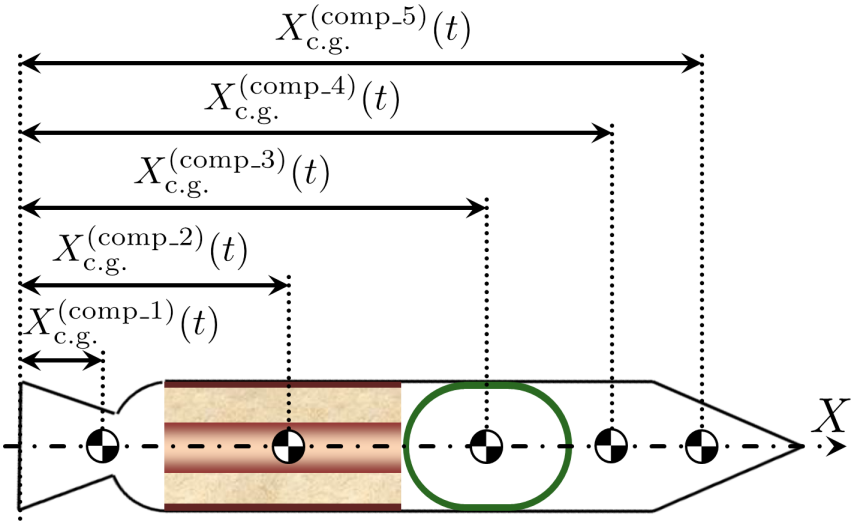

Figure 5: Definition of positions for the five-components' center of gravity.

The goal of this approach is the conception support for designers to materialize innovation. This methodology is constructed by three essences: problem definition, efficient optimization, and data mining for structurization and visualization of design space. A design problem including objective functions, design variables, and constraints, is strictly defined in view of the background physics for several months Note that problem definitions are the most important process because it directly gives effects on design space qualities. If we garrulously define a problem, unnecessary evolutionary exploration should be performed; needless mining will be also carried out because it is conceived to be low-quality design space. Then, optimization is implemented to acquire nondominated solutions[4] to become hypothetical database. Finally, data mining is implemented for this database to obtain design information. Mining has a postprocess role for optimization. Mining results might include significant knowledge for next design phase and also becomes the material to redefine a design problem.

3.1 Optimization method

DI second phase is optimization; we use evolutionary computations (ECs). Although we can employ a surrogate models[16]: the radial basis function and the Kriging model[17], which is a response surface model developed in the field of spatial statistics and geostatistics, we will not select them because they are generally difficult to deal with a large number of design variables. In addition, we would like to generate a hypothesis database using exact solutions. We also employ ECs so that plural individuals are parallel conducted. We use a hybrid EC between the differential evolution (DE) and the genetic algorithm (GA)[18].

First, multiple individuals are generated randomly as an initial population. Then, objective functions are evaluated for each individual. The population size is equally divided into subpopulations between DE and GA[5]. New individual candidates generated via DE and GA are combined. The nondominated solutions in the combined population are archived in common. Note that only the archive data is in common between DE and GA. The respective optimization methods are independently performed in the hybrid EC.

The hybrid EC is a real-coded optimizer[19]. Although GA is based on the real-coded NSGA-II (the elitist nondominated sorting genetic algorithm)[20], it is made several improvements on to be progressed with the diversity of solutions. Fonseca's Pareto ranking[21] and the crowding distance[20] are used for fitness values. The stochastic universal sampling[22] is employed for parents selection. Crossover rate is 100%; the principal component analysis blended crossover-α (PCABLX)[23] and the confidence interval based crossover using L_2 norm (CIX)[24] are used because of the high performance for convergence and diversity as well as the strength for noise[18]. The subpopulation size served by GA is equally divided for these two crossovers. Mutation rate is set to be constant as the reciprocal of the number of design variables. For alternation of generations, we employ a cross-generational elitist selection model, which uses the crowding distance for clustering; it selects N solutions from all parents and offspring. Thereupon, candidates of the next generation are $2N$. The fitness of the region that individuals congregate because of falling into local optimum and s on is estimated to be low for diversity maintaining. DE is used as the revised scheme[25] for multiobjective optimization from DE/rand/1/bin scheme. The scaling factor F is set to be 0.5. The hybrid EC has a range-adaptation function[26], which changes the search region according to the statistics of better

[4]quasi-Pareto solutions.

[5]although sub-population size can be changed at every generations on the optimizer, the determined initial sub-populations are fixed at all generations.

solutions, for all design variables. Range adaptations are implemented at every 20 generations.

3.2 Data mining

DI third phase is data mining. Scatterplot matrix (SPM)[27] or be simply named scatterplots remains one of the general visual descriptions for multidimensional data due to its simplicity. SPM is available to simultaneously visualize multidimensional data constructed by all of objective functions and design variables like as a bird's-eye view. Other data-mining techniques which have flexibility and effective visual expressiveness exist. However, we merely select SPM so that we will obtain first-step design information via observing design-space overview.

4 RESULTS

4.1 Optimization results

The population size is set to be 18 in one generation; the EC is performed until 4,000 generations. Population size of 18 is determined as a small number of the order of 10^1 because the generation number will be earned as much in evolution. The generation number is decided by evolution convergence. Plots of acquired nondominated solutions are shown in Fig. 6(a); two discontinuous connecting and convex nondominated surfaces except several isolated individuals are generated.

The tradeoffs are identical to the previous study [6]; the difference whether extinction-reignition is considered will be explained here. The essential difference between the previous and the present results is to break the upper limit of T_d and to expand it approximately 14%. This result indicates that extinction-reignition fulfills the hovering in the lower thermosphere. Extension of T_d accompanies the increase of $M_{\text{tot}}(0)$. R_d is not, however, improved due to extinction-reignition. This fact suggests that the significant design variable might not be $t_{\text{burn}}^{(\text{2nd})}$ but t_{ext}. When $t_{\text{burn}}^{(\text{2nd})}$ will serve functions, vehicles move away from the lower thermosphere; both of R_d and T_d are not increased.

If thrust direction can be horizontally controlled, $t_{\text{burn}}^{(\text{2nd})}$ is expected to give an effect on raising R_d and T_d simultaneously. Since thrust direction corresponds to body axis shown in Fig. 4 due to considering 3DoF equations of motion , $t_{\text{burn}}^{(\text{2nd})}$ is not performed functions; only t_{ext} gives an effect on T_d. However, since detailed functions of design variables are not indicated from the optimization, data mining has essential role in DI.

4.2 Data mining results

Figure 7 shows the generated SPM so that data mining is implemented. The objective is to reveal design-variable roles in the design space via observing their behaviors. SPM does not indicate the tradeoff relations among more than the optimization results shown in Fig. 6 due to identical information.

4.2.1 Knowledge for R_d

First, we will investigate design-variable roles for R_d. The optimization results shown in Fig. 6 indicate that R_d is not improved despite extinction-reignition implementation; we will trace the physical mechanism of it. SPM shown in Fig. 7 indicates effective design variables: $\dot{m}_{\text{ox}}(0)$, L_{fuel}, and $\phi(0)$.

R_d-$\dot{m}_{\text{ox}}(0)$ plot in Fig. 7 reveals a nonlinear and positive correlation between them; $\dot{m}_{\text{ox}}(0)$ gives an effect on R_d increase. $\dot{m}_{\text{ox}}(0)$ rise gives an effect on $\dot{r}_{\text{port}}(t)$ growth and thrust gain;

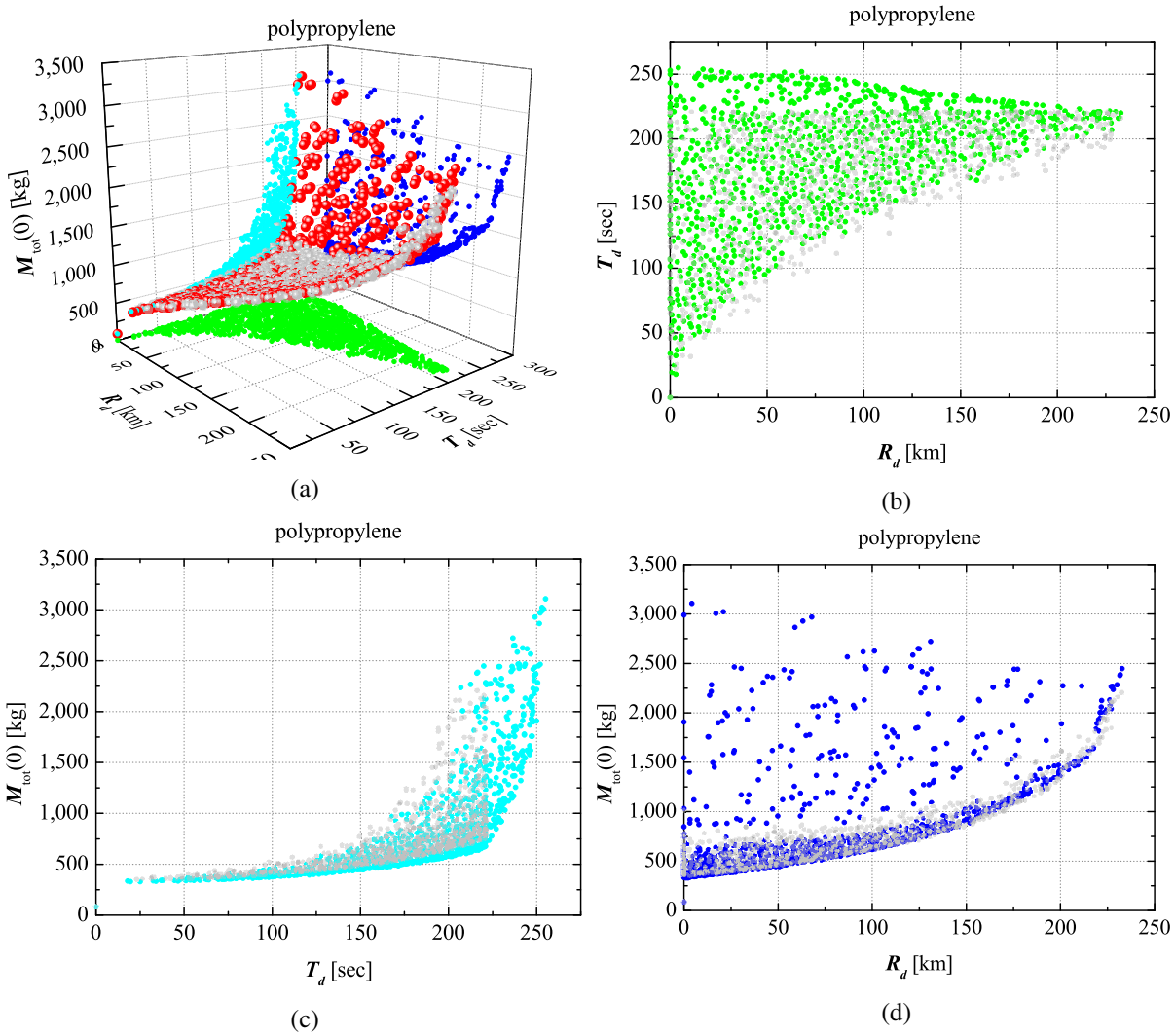

Figure 6: Plots of nondominated solutions derived by optimization, (a) plotted in the three-dimensional objective-function space (red) and their plots projected onto two dimensions, (b) plots projected onto two dimension between R_d (obj1) and T_d (obj2) (light green), (c) plots projected onto two dimension between T_d (obj2) and $M_{\rm tot}(0)$ (obj3) (light blue), and (d) plots projected onto two dimension between R_d (obj1) and $M_{\rm tot}(0)$ (obj3) (blue). Note that gray-colored plots represent the results of previous work[6] in view of no extinction-reignition.

this correlation is reasonable. However, this plot also indicates that $\dot{m}_{\rm ox}(0)$ reaches the upper limit shown in Table 1. Since this upper value descends from technical limit, $\dot{m}_{\rm ox}(0)$ is the bottleneck to realize the strategy to grow R_d as horizontal flight path in the lower thermosphere using low $\phi(0)$.

R_d-$L_{\rm fuel}$ plot in Fig. 7 similarly shows a nonlinear and positive correlation between them; $L_{\rm fuel}$ also gives an effect on R_d swell. However, $L_{\rm fuel}$ does not attain the upper limit of the design-variable space; the region to be close to $L_{\rm fuel}$ upper limit (from roughly 8 to 10 [m]) has no nondominated solution. If $L_{\rm fuel}$ increases, fuel mass rises; long-time combustion can be performed. But

- R_d-$t_{\rm burn}^{\rm (1st)}$ plot in Fig. 7 indicates that $t_{\rm burn}^{\rm (1st)}$ is not set to be close to upper limit.
- R_d-$t_{\rm burn}^{\rm (total)}$ plot in Fig. 7 reveals that $t_{\rm burn}^{\rm (total)}$ merely uses the lower half region.

That is, if $t_{\rm burn}^{\rm (1st)}$ is set over the maximum value in $t_{\rm burn}^{\rm (1st)}$ plots in Fig. 7, long combustion does not give an effect on R_d growth. Furthermore, if $t_{\rm burn}^{\rm (total)} < t_{\rm burn}^{\rm (1st)}$, we define Eq. (2); 2nd combustion

is not implemented. Thereupon, the absolute behavior of

$$t_{\text{burn}}^{(\text{2nd})} = t_{\text{burn}}^{(\text{total})} - t_{\text{burn}}^{(\text{1st})} > 0 \tag{10}$$

signifies that the hybrid EC evolves to strictly perform 2nd combustion. Thrust direction corresponds to body axis shown in Fig. 4. Body axis is diagonally downward although it depends on elevation. Therefore, if $t_{\text{burn}}^{(\text{2nd})}$ is long, a vehicle might deviate from the lower thermosphere. We consider two ways to fulfill a horizontal slide because of expanding R_d and T_d.

- We have a way to employ vectored thrust. But since there is an upper limit of deflection angle, we cannot drastically implement it. Moreover, we are difficult to control deflection angle.
- We can consider several manners not to use vectored thrust; thrust direction keeps corresponding to body axis.
    1. $\phi(0)$ is set to be as low as possible so that horizontal launch is realized, i.e., horizontal component of thrust augments. However, since $\dot{m}_{\text{ox}}(0)$ reach the upper limit, a vehicle might not attain the lower thermosphere shown in R_d-$\phi(0)$ plot in Fig. 7.
    2. We control thrust so that it balances with vertical component due to rocket weight. If we control $\dot{m}_{\text{ox}}(t)$ for 2nd combustion, this manner might be fulfilled because present $\dot{m}_{\text{ox}}(0)$ is defined as constant shown in Eq. (1).
    3. Reignitions are discontinuously and repeatedly implemented for short time. But many-time ignition might be technically difficult.

    Feasibility studies regarding above 2nd manner should be quickly investigated.

R_d-$\phi(0)$ plot in Fig. 7 indicates a linear and negative correlation between them; $\phi(0)$ decrease gives an effect on R_d augmentation. If $\phi(0)$ is low, flight path becomes horizontal; R_d increases. However, $\phi(0)$ does not reach lower limit. This is because a vehicle might not attain the lower thermosphere when $\phi(0)$ is set to be under the minimum value: roughly 63 [deg].

If we consider knowledge for setting design variables summarized hereinbefore, an effective strategy to expand R_d is that nearly vertical $\phi(0)$ is set so that a vehicle injection is implemented to the lower thermosphere; appropriate thrust is generated for 2nd combustion to horizontally move a body. If strictly vertical elevation: $\phi(0)$=90 [deg] is set, horizontal component of body velocity becomes zero, a rocket cannot have horizontal slide because thrust direction corresponds to body axis.

4.2.2 Knowledge for T_d

Second, we will consider design-variable roles for T_d. Since the optimization results shown in Fig. 6 already indicates that we can extend T_d, physical mechanisms of it will be revealed via SPM. Figure 7 indicates the effective design variables: $\dot{m}_{\text{ox}}(0)$, L_{fuel}, $t_{\text{burn}}^{(\text{total})}$, $t_{\text{burn}}^{(\text{1st})}$, t_{ext}, and $\phi(0)$. Since $\dot{m}_{\text{ox}}(0)$ and L_{fuel} have similar effects for R_d, we will consider the roles of $t_{\text{burn}}^{(\text{total})}$, $t_{\text{burn}}^{(\text{1st})}$, t_{ext}, and $\phi(0)$ hereinafter. We especially focus extended feasible region due to extinction-reignition.

T_d-$t_{\text{burn}}^{(\text{1st})}$ plot in Fig. 7 describes positive correlation between them. Summit altitude becomes near 150 [km] as $t_{\text{burn}}^{(\text{1st})}$ is larger. $\phi(0)$ is also close to be vertical to efficiently implement. But if $t_{\text{burn}}^{(\text{1st})}$ is set to be roughly full time, a hull might go over altitude of 150 [km]; we observe maximum $t_{\text{burn}}^{(\text{1st})}$ on this plot. If $\phi(0)$ is close to the lower limit: 60 [deg], summit altitude does not reach 150 [km]; T_d is not longer than that under vertical launch condition. R_d is not also

expanded. Thereupon, $\phi(0)$ is set to be vertically so that fuel mass is restrained; $M_{\rm tot}(0)$ (obj3) will be reduced on the hybrid EC.

Furthermore, if $t_{\rm burn}^{\rm (2nd)}$ is set to be long, a vehicle also goes over altitude of 150 [km] because $t_{\rm burn}^{\rm (2nd)}$ (denoted as dv* in Fig. 7) is merely set to be low value on T_d-$t_{\rm burn}^{\rm (2nd)}$ plot in Fig. 7. That is, $t_{\rm burn}^{\rm (1st)}$ is appropriately determined first to reach the lower thermosphere; $t_{\rm burn}^{\rm (total)}$ is decided not to go beyond 150 [km]. Indeed we obtain infeasible region in upper area where no individual exists on $t_{\rm burn}^{\rm (total)}$ plots in Fig. 7 although we observe strongly positive correlation between $t_{\rm burn}^{\rm (total)}$ and $t_{\rm burn}^{\rm (1st)}$ shown in Fig. 7.

Physical mechanisms regarding combustion-time behaviors mentioned above will be considered. The range of dv* is from 0 to 20 [sec], i.e., T_d-$t_{\rm burn}^{\rm (2nd)}$ plot in Fig. 7 indicates that $t_{\rm burn}^{\rm (2nd)}$ absolutely fulfills Eq. 10 condition to become a nondominated solution. This problem likes to actively employ 2nd combustion. However, $t_{\rm burn}^{\rm (2nd)}$ does not like to set to be long because a hull might go over altitude of 150 [km]. If $t_{\rm burn}^{\rm (2nd)}$ is increased, T_d linearly extends. However, there is the maximum $t_{\rm burn}^{\rm (2nd)}$: roughly 5 [sec]. This result indicates that properties of 1st and 2nd combustions are absolutely different.

- 1st needs powerful combustion to launch a body to the lower thermosphere.
- 2nd requires feeble combustion to merely sustain vehicle gross weight.

We should define $\dot{m}_{\rm ox}$ for 2nd combustion to simulate different properties and to realize a feeble 2nd combustion.

T_d-$t_{\rm ext}$ plot in Fig. 7 has the roughly linear and positive correlation. Since a vehicle draws roughly parabolic flight path, it is an efficiently operation that reignition is implemented after passing summit altitude and at the timing immediately before going down altitude of 90 [km]; this correlation is reasonable.

T_d-$\phi(0)$ plot in Fig. 7 expresses that T_d becomes large as $\phi(0)$ is close to 90 [deg]. If $\phi(0)$ becomes the vertical condition, a rocket can use entire region of the lower thermosphere from 90 to 150 [km] taking advantage of 2nd combustion; T_d is inevitably extended.

4.2.3 Knowledge for $M_{\rm tot}(0)$

$\dot{m}_{\rm ox}(0)$ has a peculiarity for $M_{\rm tot}(0)$ on their plot in Fig. 7; $M_{\rm tot}(0)$-$\dot{m}_{\rm ox}(0)$ plot shows two belts with different inclination $\mathrm{d}\dot{m}_{\rm ox}(0)/\mathrm{d}M_{\rm tot}(0)$. SPM indicates that high $\mathrm{d}\dot{m}_{\rm ox}(0)/\mathrm{d}M_{\rm tot}(0)$ is the cluster to perform long $t_{\rm ext}$ and short $t_{\rm burn}^{\rm (2nd)}$ (condition I); low $\mathrm{d}\dot{m}_{\rm ox}(0)/\mathrm{d}M_{\rm tot}(0)$ is the cluster to implement short $t_{\rm ext}$ and long $t_{\rm burn}^{\rm (2nd)}$ (condition II). Note that entire nondominated solutions in both clusters do not exist in the novel feasible region where extinction-reignition generates. If $M_{\rm tot}(0)$ is identical, we need more $\dot{m}_{\rm ox}(0)$ for a long $t_{\rm ext}$ sequence than for a short $t_{\rm ext}$ one. Because we require extra-thrust for extinction to convey fuel and oxidizer masses which burn down if we operate under no extinction-reignition condition. Thereupon, the difference of sensitivity

$$\left.\frac{\mathrm{d}\dot{m}_{\rm ox}(0)}{\mathrm{d}M_{\rm tot}(0)}\right|_{\rm condition\ I} > \left.\frac{\mathrm{d}\dot{m}_{\rm ox}(0)}{\mathrm{d}M_{\rm tot}(0)}\right|_{\rm condition\ II} \tag{11}$$

is strictly emerged. The fact indicates that vehicle gross weight with extinction-reignition swells rather than that with single-time ignition so that we actively adopt extinction-reignition to increase R_d and T_d.

Although $M_{\rm tot}(0)$-$L_{\rm fuel}$ plot in Fig. 7 shows curved surface on the plots, these are divided into two clusters that we mentioned the above; each cluster has linear correlation between $M_{\rm tot}(0)$

and L_{fuel}. If L_{fuel} shortens, fuel mass decreases; since weight for reduced fuel mass lightens, this is physically reasonable result.

4.2.4 Other knowledge

Figure 7 also indicates design variable behaviors. Especially note that there is a strong positive correlation between $\dot{m}_{\mathrm{ox}}(0)$ and L_{fuel}. This result suggests that since $\dot{m}_{\mathrm{ox}}(0)$ arrives the upper limit 30 [kg/sec] shown in Table 1, L_{fuel} cannot reach the upper limit 10 [m] due to the strong correlation; accordingly this is one of the reason not to increase $t_{\mathrm{burn}}^{(\mathrm{total})}$. The shortcoming of HREs is low $\dot{r}_{\mathrm{port}}(t)$. $\dot{r}_{\mathrm{port}}(t)$ is the function described by $\dot{m}_{\mathrm{ox}}(t)$. The improvement of $\dot{m}_{\mathrm{ox}}(0)$ is essential work to effectively use extinction-reignition and to develop impressive hybrid rocket system.

Lowest value of L_{fuel} is observed to set to be 1.0 [m] on, e.g., $M_{\mathrm{tot}}(0)$-L_{fuel} plot in Fig. 7. If $L_{\mathrm{fuel}} = 1.0$ [m], $M_{\mathrm{tot}}(0))$ minimization is fulfilled whereas $R_d = 0$ and $T_d = 0$; an individual with $L_{\mathrm{fuel}} = 1.0$ [m] belongs to a nondominated solution. The lower limit of L_{fuel} to realize $R_d \neq 0$ and $T_d \neq 0$ is confirmed to be roughly 2.8 [m], which is the absolute minimum length to reach the lower thermosphere.

Figure 7 indicates that $r_{\mathrm{port}}(0)$ is not flexible; it has roughly constant. If we set a small $r_{\mathrm{port}}(0)$, we cannot implement sufficient oxidizer mass flow to fulfill appropriate thrust. In contrast, if we set a large $r_{\mathrm{port}}(0)$, fuel mass becomes insufficient. Being proportionate to a large $r_{\mathrm{port}}(0)$ cannot basically achieve $\dot{m}_{\mathrm{ox}}(0)$.

$P_{\mathrm{cc}}(0)$ is observed as an independent design variable on Fig. 7 because it is used to decide tanks' thicknesses. In addition, Fig. 7 shows the maximum $P_{\mathrm{cc}}(0)$ is approximately 4.9 [MPa]; upper design space for $P_{\mathrm{cc}}(0)$ is not completely used. Since tanks' thickness is huge as $P_{\mathrm{cc}}(0)$ is large, vehicles might not be existable for physical reasons: heavy $M_{\mathrm{tot}}(0)$ and large drag due to small aspect ratio of body.

There is a tendency that ϵ becomes large to gain thrust. Although ϵ likes to set to be the upper limit 8.0 [-] shown in Table 1, ϵ does not directly give effects on all objective functions: R_d, T_d, and $M_{\mathrm{tot}}(0)$.

5 CONCLUSIONS

Visualizing design space has been implemented for research and development of a single-stage sounding launch vehicle with hybrid rocket engine via design informatics, which manages a hybrid evolutionary computation for multidisciplinary design optimization and a scatter plot matrix for data mining. Especial objective of this study is to reveal extinction-reignition ascendancy in a hybrid rocket engine. The optimization result consequently indicates that extinction-reignition expands duration despite no improvement of downrange in the lower thermosphere. Furthermore, data-mining result reveals the intimate knowledge regarding physical mechanisms of the objective-function behavior and of design-variable roles in design space.

ACKNOWLEDGEMENTS

This work is progressed via the discussion in the hybrid rocket research working group in ISAS/JAXA. We employed the interactive Scatter Plot Matrix; it was developed by ISAS/JAXA under Industrial Innovation R&D Topic 4 on High Performance Computing Initiative Field 4.

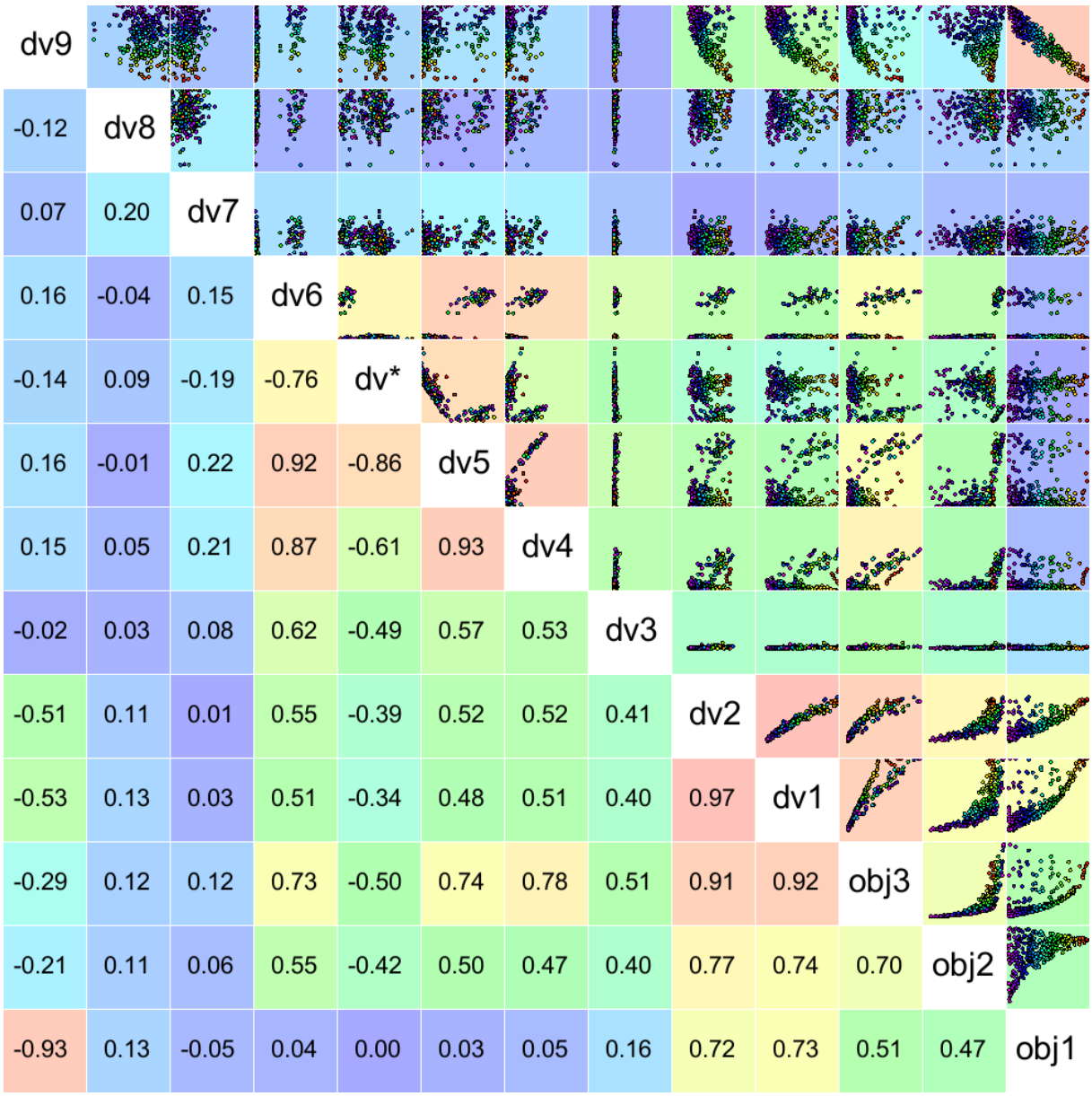

Figure 7: Scatterplots of the optimization results and their correlation coefficients. The upper/lower values of the axes of the design variables on graphs are set to be the upper/lower limits of each design variables shown in Table 1. Plots are colored by R_d as obj1; each block is colored by the absolute value of their correlation coefficients. "dv*" denotes dv4−dv5, i.e., $t_{\mathrm{burn}}^{(\mathrm{2nd})}$; dv* range is from 0 to 20 [sec].

REFERENCES

[1] M. A. Karabeyoglu, Advanced hybrid rockets for future space launch, in: Proceedings on 5th European Conference for Aeronautics and Space Sciences, EUCASS, 2013.

[2] L. Simurda, G. Zilliac, C. Zaseck, High performance hybrid propulsion system for small satellites, in: AIAA Paper 2013-3635, AIAA, 2013.

[3] M. A. Karabeyoglu, D. Altman, B. J. Cantwell, Combustion of liquefying hybrid propellants: Part 1, general theory, Journal of Propulsion and Power 18 (3) (2002) 610–620.

[4] M. A. Saraniero, L. H. Caveny, M. Summerfield, Restart transients of hybrid rocket engines, Journal of Spacecraft and Rockets 10 (3) (1973) 215–217.

[5] K. Chiba, M. Kanazaki, M. Nakamiya, K. Kitagawa, T. Shimada, Conceptual design of single-stage launch vehicle with hybrid rocket engine for scientific observation using design informatics, Journal of Space Engineering 6 (1) (2013) 15–27.

[6] K. Chiba, M. Kanazaki, M. Nakamiya, K. Kitagawa, T. Shimada, Diversity of design knowledge for launch vehicle in view of fuels on hybrid rocket engine, Journal of Advanced Mechanical Design, Systems, and Manufacturing 8 (3) (2014) JAMDSM0023, 1–14.

[7] Y. Kosugi, A. Oyama, K. Fujii, M. Kanazaki, Multidisciplinary and multi-objective design exploration methodology for conceptual design of a hybrid rocket, in: AIAA Paper 2011-1634, AIAA, 2011.

[8] S. Gordon, B. J. McBride, Computer program for calculation of complex chemical equilibrium compositions and applications I. analysis, in: NASA Reference Publication RP-1311, NASA, 1994.

[9] K. Hirata, C. Sezaki, S. Yuasa, N. Shiraishi, T. Sakurai, Fuel regression rate behavior for various fuels in swirling-oxidizer-flow-type hybrid rocket engines, in: AIAA Paper 2011-5677, AIAA, 2011.

[10] S. Yuasa, N. Shiraishi, K. Hirata, Controlling parameters for fuel regression rate of swirling-oxidizer-flow-type hybrid rocket engine, in: AIAA Paper 2012-4106, AIAA, 2012.

[11] K. Chiba, M. Kanazaki, A. Ariyarit, H. Yoda, S. Ito, K. Kitagawa, T. Shimada, Multidisciplinary design exploration of sounding launch vehicle using hybrid rocket engine in view of ballistic performance, International Journal of Turbo and Jet Engines 32 (3) (2015) 299–304.

[12] A. Arias-Montano, C. A. C. Coello, E. Mezura-Montes, Multiobjective evolutionary algorithms in aeronautical and aerospace engineering, IEEE Transactions on Evolutionary Computation 16 (5) (2012) 662–694.

[13] K. Chiba, S. Obayashi, K. Nakahashi, Design exploration of aerodynamic wing shape for reusable launch vehicle flyback booster, Journal of Aircraft 43 (3) (2006) 832–836.

[14] K. Chiba, S. Obayashi, Knowledge discovery in aerodynamic design space for flyback-booster wing using data mining, Journal of Spacecraft and Rockets 45 (5) (2008) 975–987.

[15] K. Chiba, Y. Makino, T. Takatoya, Design-informatics approach for intimate configuration of silent supersonic technology demonstrator, Journal of Aircraft 49 (5) (2012) 1200–1211.

[16] A. J. Keane, Statistical improvement criteria for use in multiobjective design optimization, AIAA Journal 44 (4) (2006) 879–891.

[17] S. Jeong, M. Murayama, K. Yamamoto, Efficient optimization design method using kriging model, Journal of Aircraft 42 (2) (2005) 413–420.

[18] K. Chiba, Evolutionary hybrid computation in view of design information by data mining, in: Proceedings on IEEE Congress on Evolutionary Computation, IEEE, 2013, pp. 3387–3394.

[19] A. Oyama, S. Obayashi, T. Nakamura, Real-coded adaptive range genetic algorithm applied to transonic wing optimization, Applied Soft Computing 1 (3) (2001) 179–187.

[20] K. Deb, A. Pratap, S. Agarwal, T. Meyarivan, A fast and elitist multiobjective genetic algorithm: NSGA-II, IEEE Transactions on Evolutionary Computation 6 (2) (2002) 182–197.

[21] C. M. Fonseca, P. J. Fleming, Genetic algorithms for multiobjective optimization: Formulation, discussion and generalization, in: Proceedings of the Fifth International Conference on Genetic Algorithms, Morgan Kaufmann, 1993, pp. 416–423.

[22] J. E. Baker, Adaptive selection methods for genetic algorithms, in: Proceedings of the International Conference on Genetic Algorithms and their Applications, Lawrence Erlbaum Associates, 1985, pp. 101–111.

[23] M. Takahashi, H. Kita, A crossover operator using independent component analysis for real-coded genetic algorithms, in: Proceedings of IEEE Congress on Evolutionary Computation 2001, IEEE, 2001, pp. 643–649.

[24] C. Hervas-Martinez, D. Ortiz-Bayer, N. Garcia-Pedrajas, Theoretical analysis of the confidence interval based crossover for real-coded genetic algorithms, in: The 7th International Conference on Parallel Problem Solving from Nature, LNCS 2439, Springer-Verlag, Berlin Heidelberg, 2002, pp. 153–161.

[25] T. Robic, B. Filipic, DEMO: Differential evolution for multiobjective optimization, in: The 3rd International Conference on Evolutionary Multi-Criterion Optimization, LNCS 3410, Splinger-Verlag, Guanajuato, Mexico, 2005, pp. 520–533.

[26] D. Sasaki, S. Obayashi, Efficient search for trade-offs by adaptive range multi-objective genetic algorithms, Journal of Aerospace Computing, Information, and Communication 2 (1) (2005) 44–64.

[27] N. Elmqvist, P. Dragicevic, J. Fekete, Rolling the dice: Multidimensional visual exploration using scatterplot matrix navigation, IEEE Transactions on Visualization and Computer Graphics 14 (6) (2008) 1539–1548.